



**HAL**  
open science

## Effect of the adsorption pH and temperature on the parameters of the Brouers–Sotolongo models

Taher Selmi, Mongi Seffen, Alain Celzard, Vanessa Fierro

### ► To cite this version:

Taher Selmi, Mongi Seffen, Alain Celzard, Vanessa Fierro. Effect of the adsorption pH and temperature on the parameters of the Brouers–Sotolongo models. *Environmental Science and Pollution Research*, 2020, 27 (19), pp.23437-23446. 10.1007/s11356-018-3835-8 . hal-03039241

**HAL Id: hal-03039241**

**<https://hal.univ-lorraine.fr/hal-03039241>**

Submitted on 3 Dec 2020

**HAL** is a multi-disciplinary open access archive for the deposit and dissemination of scientific research documents, whether they are published or not. The documents may come from teaching and research institutions in France or abroad, or from public or private research centers.

L'archive ouverte pluridisciplinaire **HAL**, est destinée au dépôt et à la diffusion de documents scientifiques de niveau recherche, publiés ou non, émanant des établissements d'enseignement et de recherche français ou étrangers, des laboratoires publics ou privés.

# **Effect of the adsorption pH and temperature on the parameters of the Brouers-Sotolongo models**

**Taher Selmi<sup>1\*</sup>, Mongi Seffen<sup>1</sup>, Alain Celzard<sup>2</sup>, Vanessa Fierro<sup>2</sup>**

<sup>1</sup> Laboratory of Energy and Materials (LabEM). ESSTHS, BP 4011 Hammam Sousse (Sousse University-Tunisia).

<sup>2</sup> Institut Jean Lamour, UMR CNRS 7198, 27 Rue Philippe Séguin, BP 21042, 88051 Epinal Cedex 9, France

\* Corresponding author (Taher Selmi) Tel: + 216 22 284 494  
E-mail address: [taher-selmi@hotmail.com](mailto:taher-selmi@hotmail.com)

## **Abstract**

The goal of the present paper was to elucidate if – and how – the parameters of the Brouers-Sotolongo fractal BSf ( $n, \alpha$ ) kinetic model ( $\alpha$  and  $\tau_C$ ) on the one hand, and of the generalised Brouers-Sotolongo GBS isotherm model ( $a$  and  $b$ ) on the other hand, are correlated with adsorption pH and temperature. For that purpose, adsorption of aqueous solutions of two common dyes, methylene blue (MB) and methyl orange (MO) was carried out on four activated carbons (ACs) at three temperatures (25, 35 and 50°C) and three pH (2.5, 5 and 8). Adsorption kinetics and isotherms were measured, and the corresponding curves were best fitted with specific forms of the aforementioned models, and corresponding to equations known as BSf ( $1, \alpha$ ) kinetic and Brouers-Gaspard isotherm models. Correlations between all models parameters and adsorption conditions were found, bringing some information about the adsorbate-adsorbent interaction.

**Keywords:** Adsorption; activated carbon; dyes; fractal kinetics; Brouers-Gaspard isotherm; heterogeneous surface

## 1. Introduction

Adsorption is a complex process that can combine interactions of different physical and/or chemical natures between the adsorbate (solute) and the active sites of the adsorbent, including electrostatic forces and Van der Waals interactions, ligand exchange, hydrogen bonding, or hydrophobic interactions (Volesky 2007). In order to understand the adsorption phenomena, several kinetic and isotherm models have been applied. Concerning kinetics, the most well-known models are intraparticle diffusion (Weber and Morris 1963), pseudo-first order (Lagergren 1898), pseudo-second-order (Ho and McKay 1999) and Elovich (Wu et al. 2009) models. As for adsorption, Freundlich (Freundlich 1906), Langmuir (Langmuir 1918), Sips (Sips 1948) and Temkin (Temkin 1941) isotherm expressions are among the most frequently used.

However, these conventional models are based on unrealistic assumptions, such as monolayer or multilayer adsorption, one single molecule per active site, no interaction between adsorbed molecules, etc., and sometimes they give little information on the adsorbate-adsorbent system. Experimental studies by Kopelman et al. (Klymko and Kopelman 1982; Kopelman 1986) on the kinetic reaction of excitons in molecular macro-clusters (inside crystalline isotopic alloy) prepared in fractal form have shown that the rate constant depends on time, which is not expressed in classical models.

For this reason, Kopelman (Kopelman 1988) and Meilanov et al. (Meilanov et al. 2002) expressed the need of developing new kinetic and isotherm models taking into accounts the fractal porosity and the heterogeneity of adsorbate-adsorbent systems. This new approach was developed by Brouers and collaborators. In 2006, Brouers and Sotolongo-Costa (Brouers and Sotolongo-Costa 2006) developed a new kinetic fractal model called BSf ( $n, \alpha$ ) based on Hill (Jones et al. 2014), Weibull (Tonkin et al. 2014) and Tsallis (Sotolongo-Grau. O et al. 2010; Sotolongo-Grau. O et al. 2013) kinetic formulae, and taking into account the systems

fractality by using the probability function and the notion of fractional derivative (Pereira 2010). BSf ( $n, \alpha$ ) encompasses several other models, depending on the values of the parameters  $n$  and  $\alpha$ . This new fractal kinetic model was applied to pharmacokinetics (Pereira 2010), water treatment (Ben Hamissa et al. 2013), and is presently more and more employed (Al-Musawi et al. 2017; Gaspard et al. 2006; Sandro et al. 2009; Selmi et al. 2018c).

In terms of adsorption at equilibrium, Brouers et al. (Brouers et al. 2005) developed a new stochastic model called general Brouers-Sotolongo (GBS) isotherm, which is based on an empirical isotherm using Burr distribution (I.W Burr 1942; Mohan D. Pant and Headrick 2013), Weibull distribution (Tonkin et al. 2014), and a cumulative probability distribution. Brouers extended the empirical model of Langmuir to simple Brouers-Sotolongo (BS) isotherm and generalised the BS model by replacing the exponent in the Weibull function by a deformed exponential used in the formalism of non extensive thermodynamics (Robledo and Moyano 2008; Tsallis 2009). The GBS isotherm also encompasses several other models, depending on the value of its parameters  $c$  and  $a$ , and has become increasingly employed in several domains such as medical application using bacteriophages for the optimised capture of bacteria (Naidoo et al. 2012), water treatment, and adsorption in general (Brouers and Al-Musawi 2015; Ncibi et al. 2008; Ncibi and Mika 2015).

Applying the BSf and GBS models presents many advantages compared to traditional ones as they give valuable information on the adsorbent surface and on the adsorbate/adsorbent interface. The main issue is that there is little information on the parameters of BSf and GBS models. In a previous manuscript (Selmi et al. 2018c), these parameters were determined and their relationships with the physicochemical characteristics of four ACs: F200, F300, Acticarbon® and Cecalite® were clarified. The objective of the present study was to elucidate whether there is a correlation between the aforementioned parameters and pH and

temperature when studying the adsorption of two dyes: methylene blue (MB) and methyl orange (MO) onto the same ACs.

## 2. Experimental

### 2.1 Materials

Four activated carbons (ACs) were used: Filtrasorb 200 (F200) and Filtrasorb 300 (F300) from *Calgon Cooperation*, and Acticarbone® and Cecalite® from *CECA*. Complete details about those materials ACs can be found elsewhere (Selmi et al. 2018c), whereas their main relevant physicochemical characteristics, i.e., those having an effect on adsorption, are reported in Table 1. MB and MO dyes were provided by Sigma-Aldrich (purity > 85%).

Table 1 : Characteristics of the four ACs used herein (Selmi et al. 2018c): surface area ( $S_{BET}$ ), total pore volume measured by nitrogen adsorption at  $-196^{\circ}\text{C}$  ( $V_{tot}$ ), total amount of surface functional groups, and pH at the point of zero charge ( $pH_{PZC}$ ).

Activated carbon	F200	F300	Acticarbone®	Cecalite®
$S_{BET}$ (m <sup>2</sup> /g)	795	884	1014	582
$V_{tot}$ (cm <sup>3</sup> /g)	0.39	0.43	0.56	0.24
Total amount of surface functional groups (mmol/g)	1.145	0.605	1.150	0.787
$pH_{PZC}$	7.20	8.03	7.36	7.75

### 2.2 Adsorption studies

MB and MO adsorption kinetics and equilibrium isotherms were performed in batch experiments as follows: 0.3 g of AC adsorbent, used in granular form with a grain size not exceeding 1 mm, were added to 100 mL of MB or MO solution with the desired dye

concentration (0.5-80 mg/L). The initial pH was adjusted by adding of HCl (0.1 mol/L) or NaOH (0.1 mol/L) solution, and was measured using a pH meter (*pH 315i*, PROLABMAS). The AC suspensions in dye solutions were stirred magnetically and, after a given time, a sample of 4 mL was withdrawn and the residual dye concentration was determined with a UV-Vis spectrophotometer (Perkin-Elmer Lambda 35) at a wavelength of 663 nm for MB, and 464 nm for MO. Once the absorbance was measured, the liquid sample was put back into the flask in order to maintain a constant liquid volume. The amount of adsorbed dye at equilibrium,  $q_e$  (mg/g), was calculated by:

$$q_e = \frac{(C_0 - C_e)V}{m} \quad \text{Equation 1}$$

where  $C_0$  and  $C_e$  (mg/L) are the initial and equilibrium dye concentrations, respectively,  $V$  (L) is the volume of solution, and  $m$  (g) is the mass of AC.

Dyes adsorption thermodynamics parameters such as standard entropy  $\Delta S^\circ$ , enthalpy  $\Delta H^\circ$ , and free energy  $\Delta G^\circ$  were calculated from adsorption data at three temperatures: 25, 35 and 50°C, using a thermostatic bath regulated at  $\pm 1^\circ\text{C}$  and following the method reported in detail elsewhere (Enaime et al. 2017).

### 2.3 Brouers-Sotolongo kinetic (BSf) and adsorption equilibrium (GBS) models

The Brouers-Sotolongo fractal kinetic (BSf) model takes into account the adsorption process complexity (Brouers 2014a) and reads:

$$q_{n,\alpha}(t) = q_e \left[ 1 - \left( 1 + (n - 1) \left( \frac{t}{\tau_c} \right)^\alpha \right)^{\frac{-1}{(n-1)}} \right] \quad \text{Equation 2}$$

where  $\alpha$  is the fractal time exponent, which is a measure of the average energy and width of the adsorption energy distribution; it decreases when the average energy and the width of the energy distribution increase.  $n$  is a (possibly fractional, i.e., non-integer) reaction order, and

$q_{n,\alpha}(t)$  and  $q_e$  are the adsorbed amounts at any time  $t$  and at saturation, respectively.  $\tau_C$  is the characteristic time of the complex kinetics, and corresponds to the necessary time to reach equilibrium so that the BSf model can predict the equilibrium time. In relation to the parameters  $n$ ,  $\alpha$  and  $\tau_C$ , a time of half-reaction  $\tau_{1/2}$  can be determined to predict the time necessary to sorb half of the amount at equilibrium; more details are given elsewhere (Selmi et al. 2018c). Several other models can be recovered from the expression of BSf, depending on the values of  $n$  and  $\alpha$ , as shown in Table 2. More details can be found elsewhere (Brouers 2014a).

Table 2: Kinetic models derived from the BSf kinetic model

$n$	$\alpha$	Model	Expression	Eq. number	Reference
1	1	pseudo-first order (PFO)	$q_{1,1}(t) = q_{e,PFO} \left[ 1 - \text{Exp} \left( -\frac{t}{\tau_C} \right) \right]$	Eq. 3	(Lagergren 1898)
2	1	pseudo-second order (PSO)	$q_{2,1}(t) = q_{e,PSO} \left[ \frac{\frac{t}{\tau_C}}{1 + \frac{t}{\tau_C}} \right]$	Eq. 4	(Ho and McKay 1999)
1	--	Weibull	$q_{1,\alpha}(t) = q_{e,W} \left[ 1 - \text{Exp} \left( -\left( \frac{t}{\tau_C} \right)^\alpha \right) \right]$	Eq. 5	(Brouers 2014a)
2	--	Hill	$q_{2,\alpha}(t) = q_{e,H} \left[ 1 - \left( 1 + \left( \frac{t}{\tau_C} \right)^\alpha \right)^{-1} \right]$	Eq. 6	(Brouers 2014a)

The GBS isotherm model takes into account the physical and chemical heterogeneity of the adsorbent and of the adsorbate/adsorbent system (Brouers and Al-Musawi 2015). It reads:

$$q_{e \text{ GBS}} = q_{e \text{ max}} \left[ 1 - \text{Exp}_c \left( -\left( \frac{c_e}{b} \right)^a \right) \right] = q_{e \text{ max}} \left[ 1 - \left( 1 + c \left( \frac{c_e}{b} \right)^a \right)^{-1/c} \right] \quad \text{Equation 7}$$

Depending on the parameters  $a$  and  $c$ , several other models can be derived from the GBS equation, as shown in Table 3; more details can be found elsewhere (Brouers 2014b).

Table 3: Adsorption isotherms models derived from the GBS isotherm.

$c$	$a$	Model	Equation form	Eq. number	Reference
0	--	BS	$q_{e\ BS} = q_{e\ maxBS} \left[ 1 - \text{Exp} \left( - \left( \frac{C_e}{b} \right)^a \right) \right]$	Eq. 8	(Brouers 2014b)
0.5	--	BG	$q_{e\ BG} = q_{e\ maxBG} \left[ 1 - \left( 1 + \frac{1}{2} \left( \frac{C_e}{b} \right)^a \right)^{-2} \right]$	Eq. 9	(Brouers and Al-Musawi 2015)
1	--	HS	$q_{e\ HS} = q_{e\ maxHS} \left[ 1 - \left( 1 + \left( \frac{C_e}{b} \right)^a \right)^{-1} \right]$	Eq. 10	(Sips 1948)
1	1	Langmuir	$q_{e\ L} = q_{e\ maxL} \frac{C_e}{b + C_e}$	Eq. 11	(Langmuir 1918)
$C_e \ll b$		Freundlich	$q_{e\ F} = K_F C_e^a$	Eq. 12	(Freundlich 1906)

The experimental data were non-linearly fitted by using the Levenberg-Marquardt iteration algorithm supplied with OriginPro® 2016 Software.

### 3. Results and discussion

#### 3.1 Effect of initial dye concentration on adsorption kinetics

Figure 1 shows the effect of the initial concentration of MB (Fig. 1(a)) and of MO (Fig. 1(b)) on the time required for reaching the equilibrium, which increased with the initial dye concentration. As can be seen, adsorption occurred in two stages: (i) the initial adsorption stage was fast, probably due to the high number of sites available for sorption; (ii) the second phase was slower due to the fact that the number of easily accessible sites decreased and the adsorbate needed longer times to reach the last remaining adsorption sites (Kesraoui et al. 2016). As an example, the necessary time to reach the equilibrium on F300 was 50 min and 25 min when using  $C_0=5$  mg/L of MB and MO, respectively. The equilibrium time was multiplied by a factor 4 when increasing the initial dye concentration up to 80 mg/L, suggesting that adsorption was controlled by intraparticle and boundary layer diffusion

(Enaime et al. 2017). Similar results were found with the other 3 ACs (see Figures SI 1 to SI 3 of the Supplementary Information).

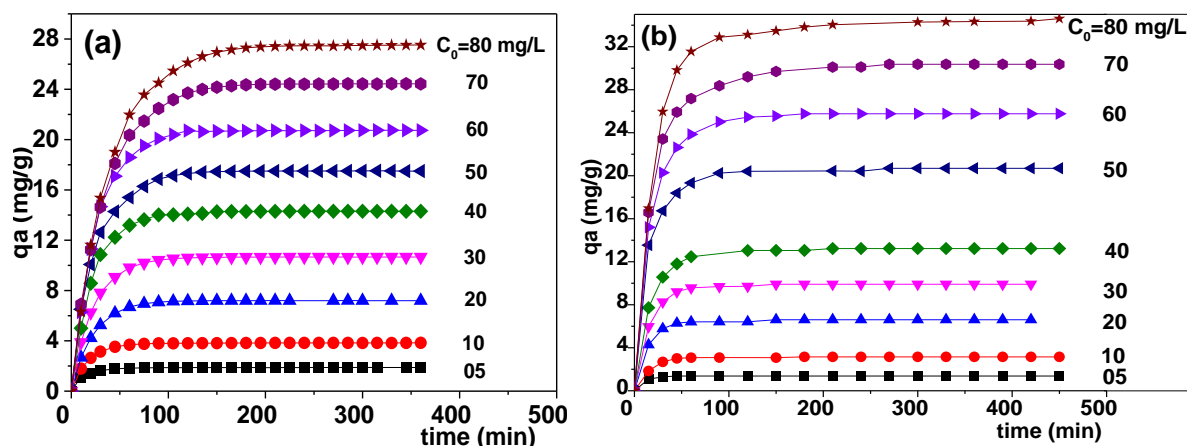


Figure 1: Effect of contact time and initial concentration on: (a) MB at pH 8; and (b) MO at pH 2.5 onto F300 at 25°C (lines are just guides for the eye).

### 3.2 Effect of initial pH and temperature on adsorption

Figure 2 and Table SI 1 shows the effect of pH and temperature on MB and MO adsorption capacities of the four ACs when the initial dye concentration  $C_0$  was fixed to 10 mg/L. These effects were investigated at pH 2.5, 5 and 8 at each temperature of 25, 35 and 50°C. MB adsorption at equilibrium onto F300 increased slightly from 3.18 to 3.39 mg/g when the pH increased from 2.5 to 8 at 25°C, indicating that MB was favourably adsorbed at basic pH. On the contrary, MO adsorption at equilibrium onto F300 decreased slightly from 3.15 to 3.00 mg/g when the pH increased from 2.5 to 8 at 25°C indicating that MO was favourably adsorbed at acidic pH. This fact is in agreement with the  $pH_{PZC}$  of F300 (8.03), suggesting that the adsorbent surface was approximately neutral at pH 8 and positively charged at pH 2.5, i.e., was attracting anions. MB is a cationic dye, and hence it is positively charged in solution and thus more adsorbed at basic pH when the surface of the carbon is not charged, than at

acidic pH when the surface of the carbon is positively charged. The opposite was observed for MO, which is an anionic dye.

Therefore, the study of the effect of temperature on adsorption onto was made by fixing the pH to 8 for MB and to 2.5 for MO. The amounts of MB and MO adsorbed onto F300 increased with temperature from 25 to 50°C from 3.39 to 3.84 mg/g for MB, and from 3.15 to 3.51 mg/g for MO (Table SI 1). The corresponding data will be examined in terms of thermodynamic parameters in the next section.

Figure 2 shows the MB and MO equilibrium adsorption capacities of the four ACs as a function of temperature and pH. All adsorbents had  $pH_{PZC}$  between 7.20 and 8.03, therefore they essentially had the same behaviour, i.e., MB adsorption was more favourable at pH 8, when the surface of the AC was nearly neutral, than at pH 2.5, when it was positively charged and thus led to higher electrostatic repulsion. On the contrary, MO adsorption was more favourable at pH 2.5 when surface of AC was positively charged and thus led to higher electrostatic attraction since MO is an anionic dye. Dissociation and electrostatic repulsion are also largely influenced by temperature (Ncibi and Mika 2015), and the same general trend was observed for the four ACs. Adsorption increased with temperature in the range 35 to 50°C.

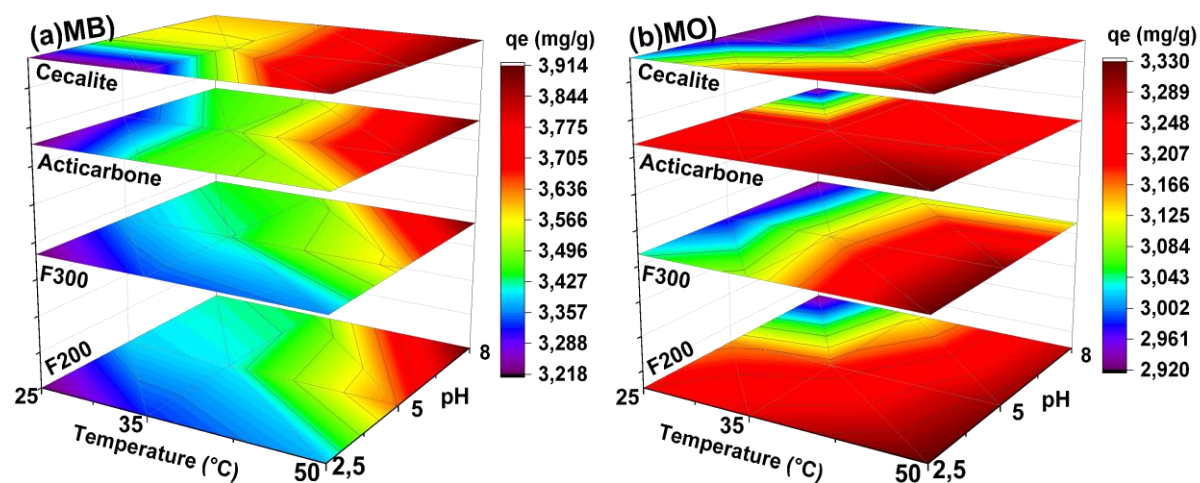


Figure 2: Effect of pH and temperature on the adsorbed amount onto ACs of: (a) MB; and (b) MO, both at  $C_0=10$  mg/L.

### 3.3 Thermodynamic analysis

Figure 3 shows the variation of standard free energy  $\Delta G^\circ$  with pH and temperature for MB and MO adsorption onto the four ACs.  $\Delta G^\circ$  was in the range from -6.00 to -20.45 kJ/mol, indicating the spontaneous nature of MB and MO adsorption onto the four materials. The absolute value of  $\Delta G^\circ$  increased with temperature, for all pH, indicating a more efficient adsorption at higher temperature. Apart from this, the absolute value of  $\Delta G^\circ$  decreased with an increase of pH for MB adsorption, whereas the opposite occurred with MO. This behaviour was clearly seen for MB adsorption at the highest temperature, but was less obvious for MO adsorption in the same conditions due to the opposite effects of pH and temperature on MO adsorption.

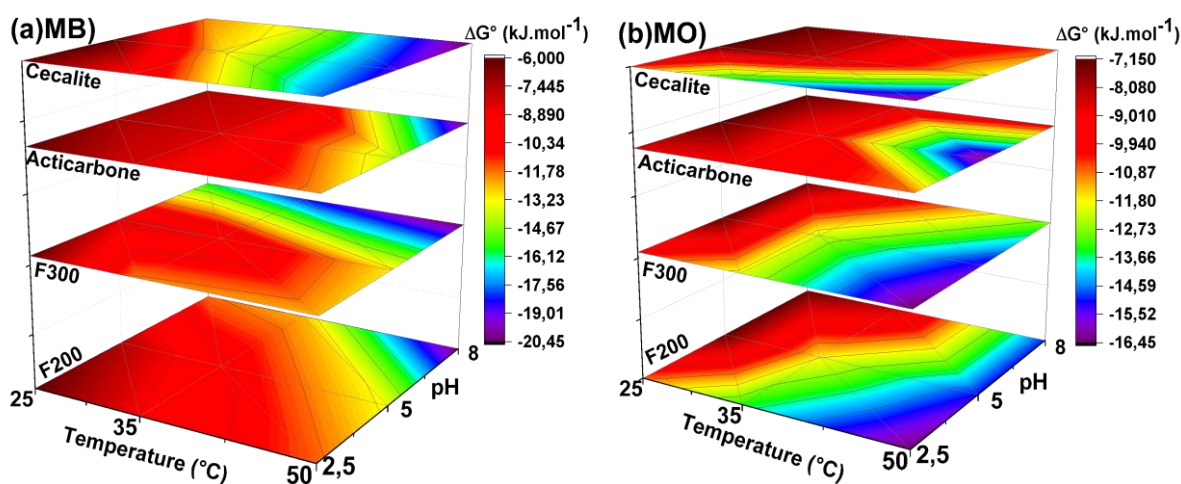


Figure 3: Effect of pH and temperature on the free energy of adsorption  $\Delta G^\circ$  onto the four ACs of: (a) MB; and (b) MO, both at  $C_0=10$  mg/L.

Figure 4 shows the variations of standard adsorption enthalpy  $\Delta H^\circ$  and of standard adsorption entropy  $\Delta S^\circ$  with pH for MB and MO adsorption onto the four ACs; the

corresponding numerical results are given in Table SI 2 of the Supplementary Information.  $\Delta H^\circ$  was always positive: it decreased when the pH was increased for the adsorption of MB, but increased with pH for the adsorption of MO onto all ACs (Figure 4 and Table SI 2 of the Supplementary Information).

$\Delta S^\circ$  was always positive and showed the same behaviour as  $\Delta H^\circ$  with pH (Figure 4 and Table SI 2 of the Supplementary Information). The positive values of  $\Delta S^\circ$  suggest an increased randomness at the AC/solution interface during the sorption process. Similar results were found by other investigators working on dye adsorption onto various adsorbents (Bouhamed et al. 2016; Enaime et al. 2017; Kesraoui et al. 2017; Selmi et al. 2018a).

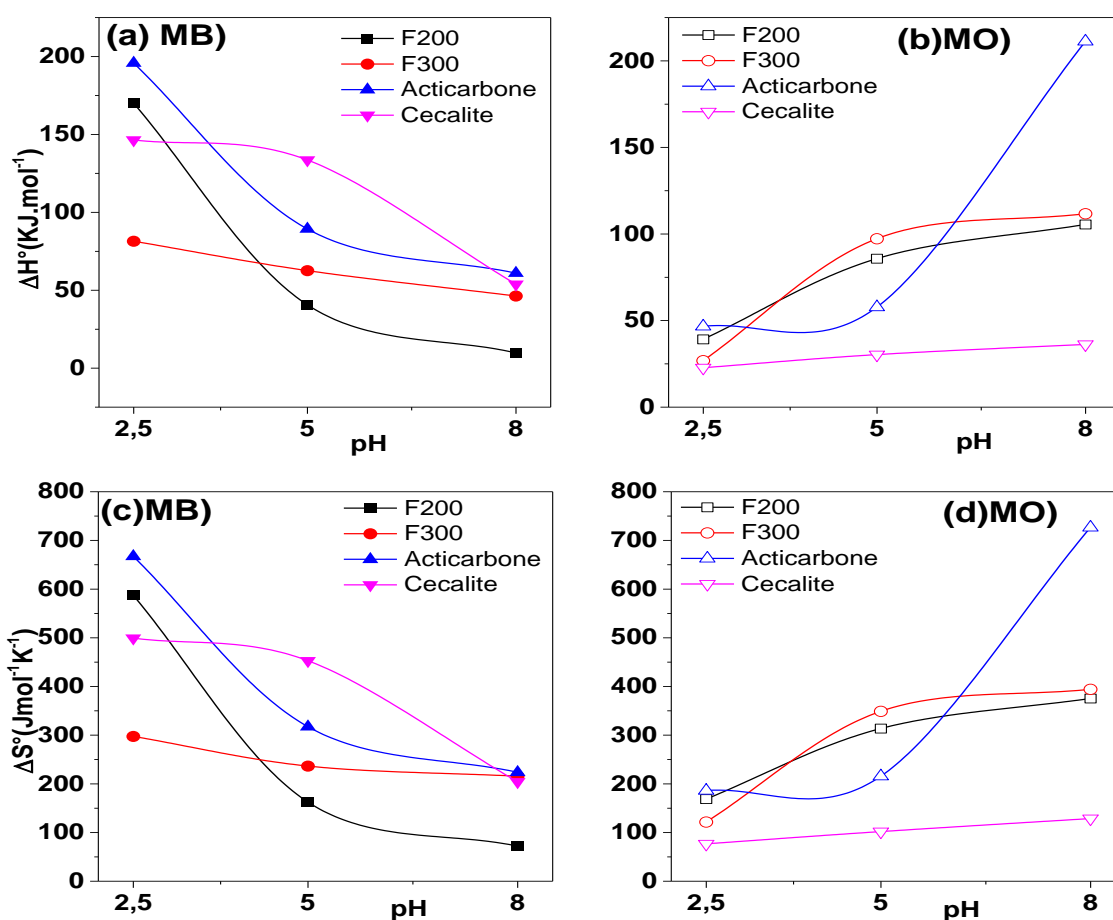


Figure 4: Effect of pH on: (a and b) standard adsorption enthalpy  $\Delta H^\circ$ ; and (c and d) on standard adsorption entropy  $\Delta S^\circ$  for: (a and c) MB; and (b and) MO onto the four ACs.

### 3.4. Kinetic data analysis

Herein, based on our former work (Selmi et al. 2018c), the reaction order  $n = 1$  was used for the BSf kinetics model because of the excellent fits it let for all ACs. The Weibull equation ( $n = 1$  and  $\alpha \neq 1$ ) was indeed the most relevant one for fitting the kinetic data, and this was in agreement also with previous studies on Indigo Carmine adsorption onto F200 (Kesraoui et al. 2017). Figure 5 shows the experimental kinetic data of MB and MO adsorption onto F300, and the corresponding non-linear fits using the BSf ( $1, \alpha$ ) model (i.e.,  $n$  was fixed to 1). The BSf ( $1, \alpha$ ) model fitted very well the experimental data and equally good results were obtained for the other three ACs, as shown in Figure SI 4 of the Supplementary Information.

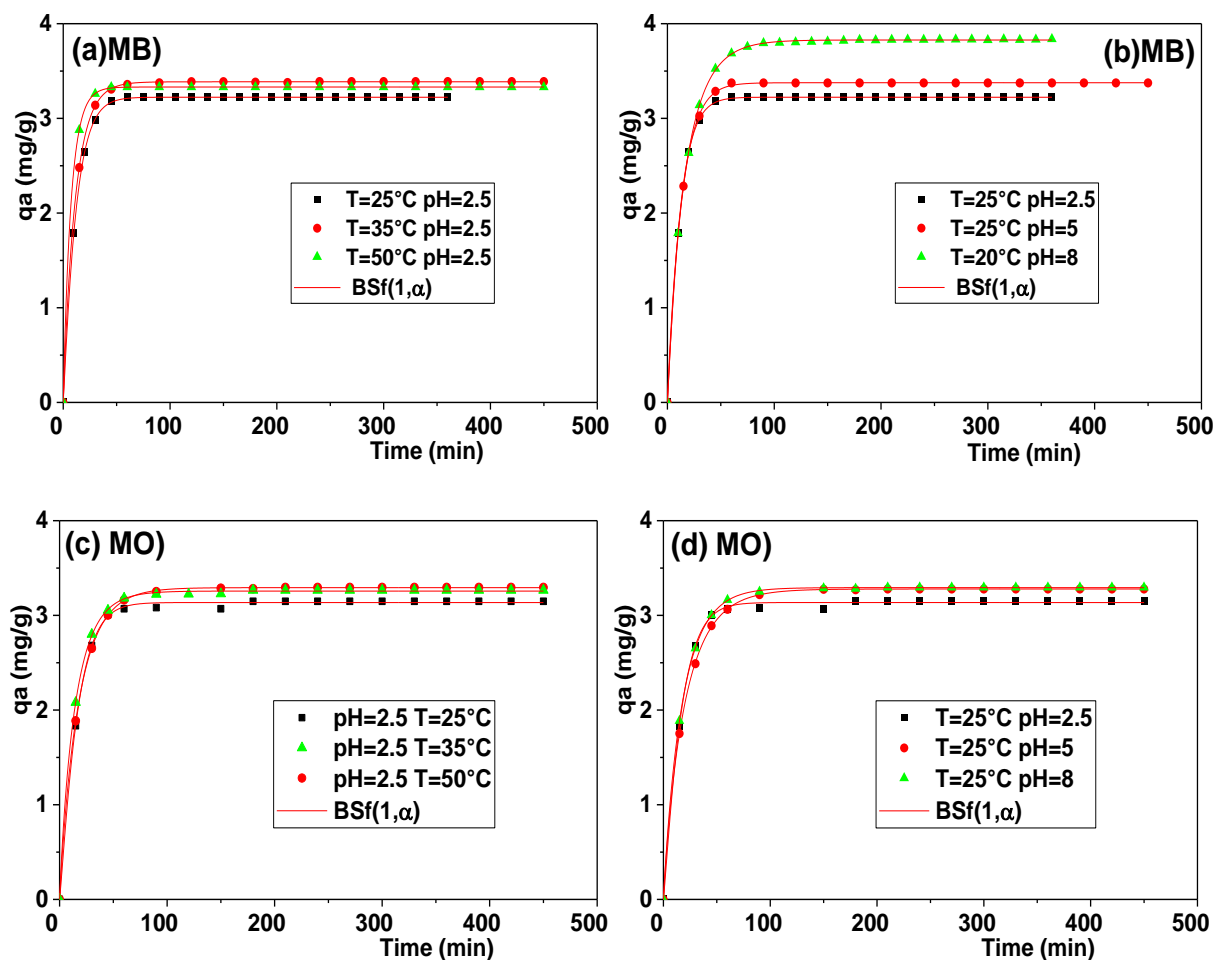


Figure 5: BSf ( $1, \alpha$ ) kinetics model applied to the adsorption of: (a,b) MB; and (c,d) MO onto F300 for different pH and temperatures, using an initial dye concentration  $C_0=10$  mg/L.

Figure 6 shows the effect of pH and temperature on the BSf ( $1, \alpha$ ) constants  $\tau_C$  and  $\alpha$  for the adsorption of MB and MO. Certain correlations between  $\tau_C$ ,  $\alpha_{MB}$ ,  $\alpha_{MO}$  with pH and temperature were observed. Tables SI 3 to SI 6 of the Supplementary Information present the BSf ( $1, \alpha$ ) parameters for the four ACs.

Previous studies (Al-Musawi et al. 2017; Ben Hamissa et al. 2013; Selmi et al. 2018b; Selmi et al. 2018c) showed that the interactions between adsorbate/adsorbent were fractal when  $\alpha$ , sometimes referred to as the global fractal time, was lower than 1.  $\alpha$  represents the memory effect produced in systems where the reaction at any time,  $t$ , depends on the history of the process.  $\alpha$  arises from the energetic and geometric heterogeneity of the adsorbent (Ben Hamissa et al. 2013). Figure 6(b) and Table SI 3 of the Supplementary Information show that the adsorption of MB onto F300 is slightly fractal ( $\alpha_{MB}$  between 0.80 and 1.12) and the adsorption of MO onto F300 is clearly fractal ( $\alpha_{MO}$  between 0.67 and 1.13). On the one hand,  $\alpha_{MB}$  increased from 0.92 to 1.07 when the pH was increased from 2.5 to 8 at 25°C, indicating that raising the pH diminished the fractal nature of the phenomena. On the other hand,  $\alpha_{MO}$  decreased from 1.13 to 0.92 when increasing the pH from 2.5 to 8 at 25°C, indicating that, instead, raising the pH promoted fractal adsorption of MO onto F300. In fact, fractal phenomena became stronger when increasing the pH at temperatures above 35°C for both MB and MO adsorption. The same results were found when studying MB adsorption onto F200 and Acticarbone®, and MO adsorption onto Acticarbone® and onto Cecalite® (see Figure SI 5 and Tables SI 4 and SI 5 of the Supplementary Information). MB adsorption onto Cecalite® deserves special attention because it is highly fractal, with a  $\alpha_{MB}$  around 0.67 on average; see Figure SI 5 and Table SI 6 of the Supplementary Information.

Since the increase of pH had a positive effect on the adsorption of MB and a negative effect on the adsorption of MO, the characteristic time decreased with pH for MB adsorption (e.g. from 16.69 to 12.14 min at 25°C for MB adsorption onto F300), and increased with pH for MO adsorption (e.g. from 16.78 to 20.16 min at 25°C for MO adsorption onto F300). The same behaviour was clearly apparent for the adsorption of MB and MO onto all other ACs (see Figure 6, and Figure SI 5 and Tables SI 3 to SI 6 of the Supplementary Information).

On the other hand, the temperature had a positive effect on both MB and MO adsorption, the increase of temperature increasing the initial rate of dye adsorption. Consequently, the characteristic time decreased with temperature. This behaviour is clearly apparent for the adsorption of MB and MO onto all ACs in Figure 6, Figure SI 5, and Tables SI 3 to SI 6 of the Supplementary Information. At favourable pH (8 for MB and 2.5 for MO), the characteristic time for the adsorption onto F300 of MB,  $\tau_{cMB}$ , and of MO,  $\tau_{cMO}$ , decreased when increasing the temperature, from 12.14 to 6.23 min and from 16.78 to 8.25 min, respectively (see Table SI 3 of the Supplementary Information). These results agree with previous studies (Ben Hamissa et al. 2013; Kesraoui et al. 2017; Selmi et al. 2018b). Increasing pH and temperature at the same time produced a decrease of the fractality degree  $\alpha$  and the adsorption became faster, reducing in turn the characteristic time,  $\tau_C$ .)

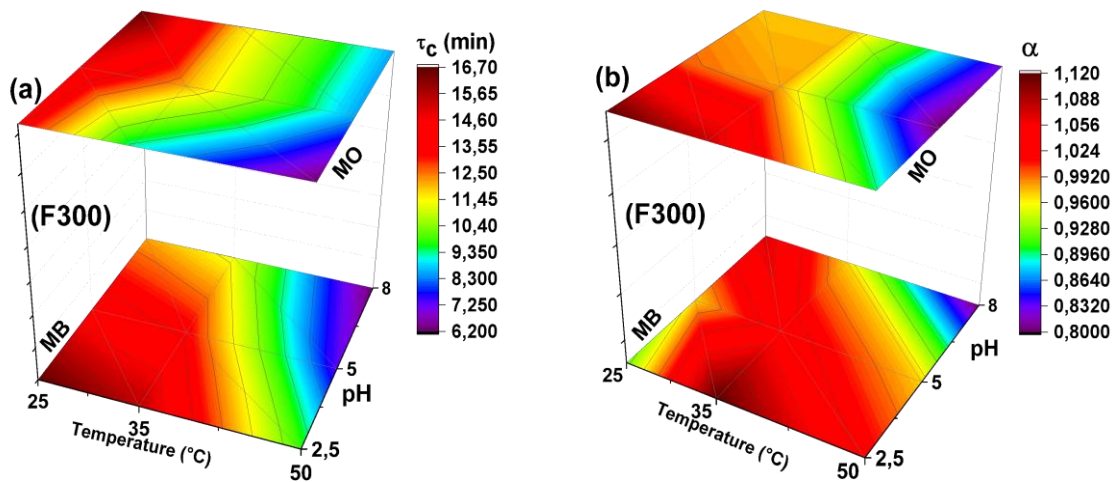


Figure 6: Variation with pH and temperature of BSf ( $1, \alpha$ ) parameters: (a)  $\tau_C$ ; and (b)  $\alpha$ , for the adsorption onto F300 of MB and MO (both at  $C_0=10$  mg/L).

### 3.5. Adsorption isotherm fitting

The GBS isotherm was used by fixing the heterogeneity degree,  $c$ , equal to 0.5, based on a previous study (Selmi et al. 2018c). And indeed, excellent fits were obtained with  $c = 0.5$ , hence the Brouers-Gaspard (BG) equation ( $a \neq 1$  and  $c = 0.5$ ) was the most relevant one for fitting the isotherm adsorption data of MB and MO onto ACs. A stochastic analysis of physicochemical reactions in complex systems (Stanislavsky and Weron 2013) showed that the exponent  $c$  is related to the cluster or aggregation organization of the system. Figure 7 shows that the experimental isotherms of MB and MO adsorbed onto F300 were very well fitted with BG equation. Equally good results were obtained for the other three ACs, and the corresponding results are given in Figure SI 6 of the Supplementary Information.

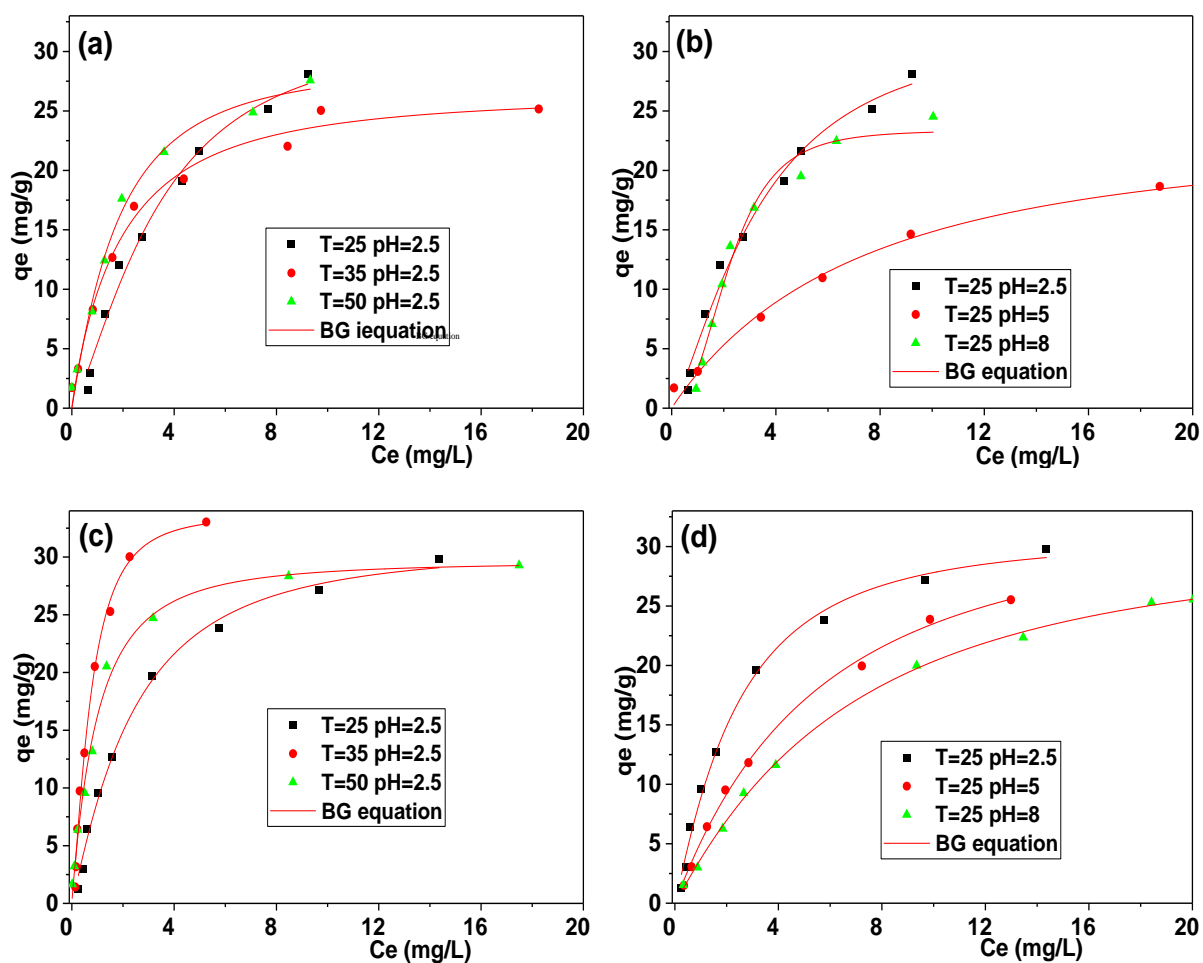


Figure 7: Fits of the BG isotherm to the adsorption data onto F300 of: (a and b) MB; and (c and d) MO, for different temperatures and pH.

Figure 8 shows the effect of pH and temperature on the BG parameters  $a$  and  $b$  for the adsorption of MB and MO, obtained from the non-linear fits of the adsorption data for all ACs. The corresponding values are listed in Tables SI 7 to SI 10 of the Supplementary Information.  $a$  and  $b$  are clearly correlated with pH and temperature. For instance,  $a$  increased with pH (from 0.48 to 0.93 at 25°C) and temperature (from 0.93 to 2.15 at pH 8), see Table SI 7, for MB adsorption onto F300. On the other hand,  $a$  decreased when increasing the pH from 2.5 to 8 (from 1.06 to 0.98 at 25°C) for MO adsorption onto F300, and increased with temperature from 25 to 50°C (from 1.06 to 1.26 at pH 2.5) due to the unfavourable effect of pH and favourable effect of temperature (Table SI 7). The same behaviours were clearly observed for the adsorption of MB and MO onto the 3 other ACs (Tables SI 8 to SI 10).

BG sorption model assumes that adsorption takes place on a heterogeneous surface with a distribution of sorption energies representative of different active sites which are progressively occupied.  $a$  represents a degree of the fractal nature of a heterogeneous system (Brouers 2014a; Brouers and Al-Musawi 2015; Brouers and Francisco 2016). When  $a > 1$ , fast initial sorption kinetics occurs, and there is probably more than one molecule sorbed by active site; when  $a < 1$ , slow initial sorption kinetics is observed. Brouers et al. (Brouers et al. 2005) showed that the exponent  $a$  is proportional to  $kT/E_s$ , where  $k$ ,  $T$  and  $E_s$  are Boltzmann constant, absolute temperature and sorption energy distribution, respectively. For a typical  $E_s$ ,  $1/a$  measures the energy distribution width, and therefore the energy heterogeneity of the surface.

The parameter  $b$  was also correlated with pH and temperature. At 25°C, the values of  $b$  related to MB and MO adsorption onto F300 decreased from 3.49 to 2.37 mg/L and increased from 2.49 to 8.74 mg/L, respectively, when increasing the pH from 2.5 to 8. At favourable pH

(8 for MB and 2.5 for MO), the  $b$  parameter of MB and MO adsorption onto F300 decreased from 2.37 to 0.20 mg/L and from 2.49 to 0.79 mg/L, respectively, when increasing the temperature from 25 to 50°C. Similar results were clearly observed for the adsorption of MB and MO onto the other three ACs (see again Tables SI 8 to SI 10 of the Supplementary Information). The increase of temperature speeds up the adsorption, so that the isotherm reaches quickly at saturation and thereafter the equilibrium concentration decreases.  $b$  is thus related to equilibrium concentration, in agreement with previous results (Selmi et al. 2018c).

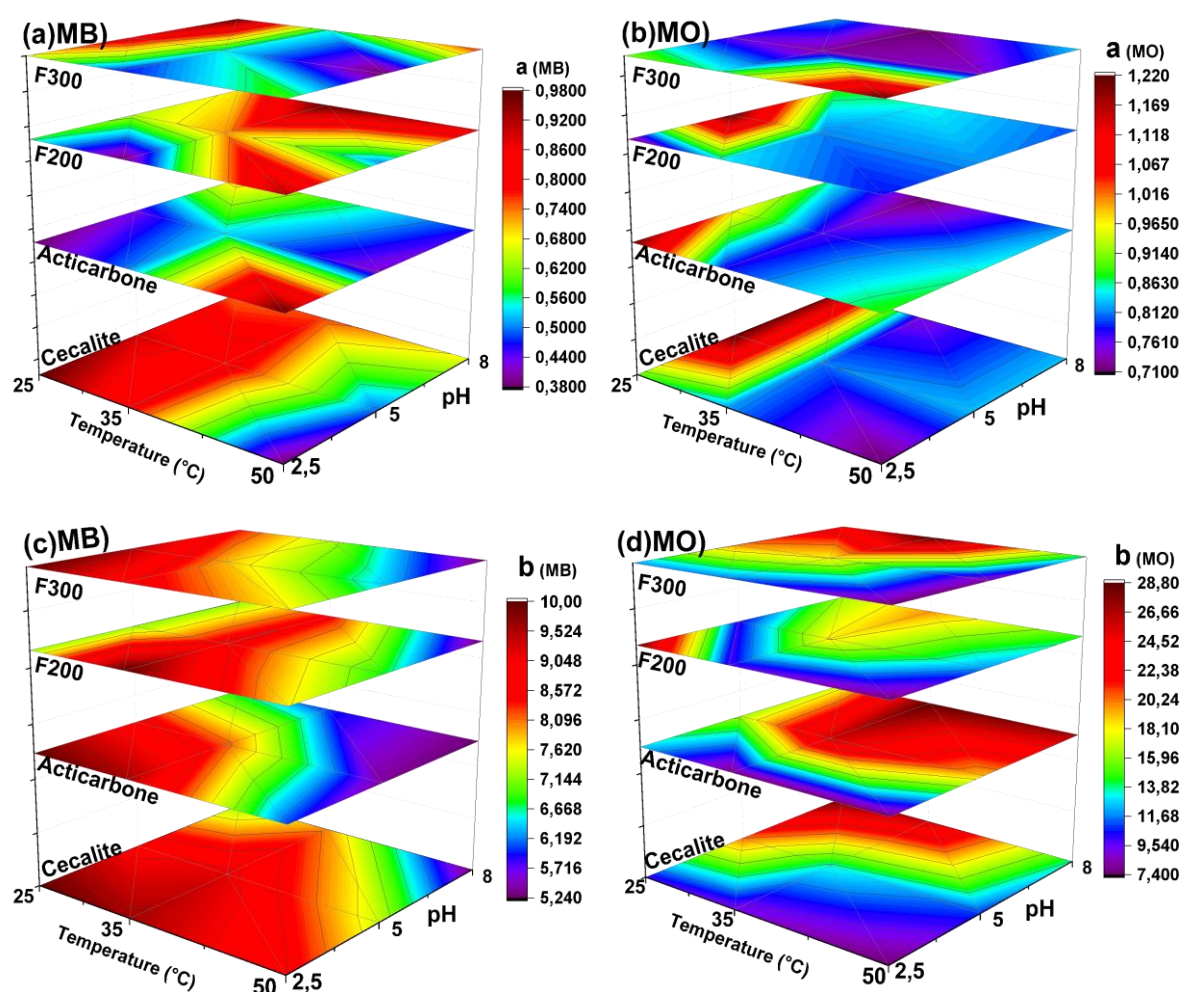


Figure 8: Variation with pH and temperature of BG parameters,  $a$  and  $b$ , determined by adsorption of: (a and c) MB; (b and d) MO, onto F200, F300, Acticarbon® and Cecalite®.

## 4. Conclusion

In this work, the adsorption of two different dyes in aqueous solution, methylene blue (MB) and methyl orange (MO), was investigated as a function of pH and temperature on four different activated carbons. The thermodynamics studies revealed that the adsorption process is spontaneous and endothermic. Both the nonlinear Brouers-Sotolongo fractal, BSf ( $n, \alpha$ ), kinetic model and the generalised Brouers-Sotolongo, GBS, isotherm model were found to fit very adequately the corresponding experimental results.

The experimental kinetic data were best described by the BSf ( $1, \alpha$ ) model involving the adsorption of MB and MO on a fractal surface of AC. The parameter  $\alpha$ , named global fractal time index, can be correlated with both pH and temperature, indicating its effects on the surface fractality and leading to the conclusion that its value comes from the assumed fractal diffusion and sorption kinetics. This is due to the energetic and geometric heterogeneity of the surface of adsorbent. The characteristic time  $\tau_C$  necessary to reach the equilibrium could also be correlated with both pH and temperature: the favourable effect of pH and temperature decreased  $\tau_C$ .

As for the data at equilibrium, the isotherms were best described by the Brouers-Gaspard (BG) model, which involves the adsorption of MB and MO onto a heterogeneous AC surface. The exponent  $a$ , which measures the energy heterogeneity of the surface, was found to be proportional to the adsorption energy distribution. The favourable effect of both pH and temperature decreased the constant  $b$  of the model, which was found to be related to equilibrium concentration.

## **Acknowledgements**

The authors gratefully acknowledges the financial support from the EU-METALIC: Erasmus Mundus project and the Tunisian Ministry of Higher Education and Scientific Research.

## References

- Al-Musawi TJ, Brouers F, Zarrabi M (2017) Kinetic modeling of antibiotic adsorption onto different nanomaterials using the Brouers–Sotolongo fractal equation *Environ Sci Pollut Res* 24:4048-4057 doi:10.1007/s11356-016-8182-z
- Ben Hamissa AM, Brouers F, Ncibi MC, Seffen M (2013) Kinetic Modeling Study on Methylene Blue Sorption onto Agave americana fibers: Fractal Kinetics and Regeneration *Studies Sep Sci Technol* 48:2834-2842 doi:10.1080/01496395.2013.809104
- Bouhamed F, Elouear Z, Bouzid J, Ouddane B (2016) Multi-component adsorption of copper, nickel and zinc from aqueous solutions onto activated carbon prepared from date stones *Environ Sci Pollut Res* 23:15801-15806 doi:10.1007/s11356-015-4400-3
- Brouers F (2014a) The fractal (BSf) kinetics equation and its approximations *J Mod Phys* 5:1594 doi:doi.org/10.4236/jmp.2014.516160
- Brouers F (2014b) Statistical foundation of empirical isotherms *Open J Stat* 4:687-701 doi:<http://dx.doi.org/10.4236/ojs.2014.49064>
- Brouers F, Al-Musawi TJ (2015) On the optimal use of isotherm models for the characterization of biosorption of lead onto algae *J Mol Liq* 212:46-51 doi:10.1016/j.molliq.2015.08.054
- Brouers F, Francisco M-M (2016) Dubinin isotherms versus the Brouers–Sotolongo family isotherms: A case study *Adsor Sci Technol* 34:552-564 doi:doi:10.1177/0263617416670909
- Brouers F, Sotolongo-Costa O (2006) Generalized fractal kinetics in complex systems (application to biophysics and biotechnology) *Phys A: Stat Mech Appl* 368:165-175 doi:<http://doi.org/10.1016/j.physa.2005.12.062>
- Brouers F, Sotolongo O, Marquez F, Pirard JP (2005) Microporous and heterogeneous surface adsorption isotherms arising from Levy distributions *Phys A: Stat Mech Appl* 349:271-282 doi:<http://doi.org/10.1016/j.physa.2004.10.032>
- Enaïme G, Ennaciri K, Ounas A, Baçaoui A, Seffen M, Selmi T, Yaacoubi A (2017) Preparation and characterization of activated carbons from olive wastes by physical and chemical activation: Application to Indigo carmine adsorption *J Mater Environ Sci* 8:4125-4137
- Freundlich H (1906) Over the adsorption in solution *J Phys Chem* 57:385-471

- Gaspard S, Altenor S, Passe-Coutrin N, Ouensanga A, Brouers F (2006) Parameters from a new kinetic equation to evaluate activated carbons efficiency for water treatment Water Res 40:3467-3477 doi:10.1016/j.watres.2006.07.018
- Ho YS, McKay G (1999) Pseudo-second order model for sorption processes Process Biochem 34:451-465 doi:[http://doi.org/10.1016/S0032-9592\(98\)00112-5](http://doi.org/10.1016/S0032-9592(98)00112-5)
- I.W Burr (1942) Cumulative Frequency Functions The Annals of Mathematical Statistics 13:215-232 doi:org/10.1214/aoms/1177731607
- Jones LB, Secomb TW, Dewhirst MW, El-Kareh AW (2014) The additive damage model: A mathematical model for cellular responses to drug combinations J Theor Biol 357:10-20 doi:<https://doi.org/10.1016/j.jtbi.2014.04.032>
- Kesraoui A, Moussa A, Ben Ali G, Seffen M (2016) Biosorption of alpacide blue from aqueous solution by lignocellulosic biomass: Luffa cylindrica fibers Environ Sci Pollut Res 23:15832-15840 doi:10.1007/s11356-015-5262-4
- Kesraoui A, Selmi T, Seffen M, Brouers F (2017) Influence of alternating current on the adsorption of indigo carmine Environ Sci Pollut Res 24:9940-9950 doi:10.1007/s11356-016-7201-4
- Klymko PW, Kopelman R (1982) Heterogeneous exciton kinetics: triplet naphthalene homofusion in an isotopic mixed crystal The Journal of Physical Chemistry 86:3686-3688 doi:10.1021/j100216a003
- Kopelman R (1986) Rate processes on fractals: Theory, simulations, and experiments Journal of Statistical Physics 42:185-200 doi:10.1007/bf01010846
- Kopelman R (1988) Fractal Reaction Kinetics Science 241:1620-1626 doi:doi.org/10.1126/science.241.4873.1620
- Lagergren S (1898) Zur Theorie der Sogenannten Adsorption Gelöster Stoffe, Kungliga Svenska Vetenskapsakade- miens Handlingar 24:1-39
- Langmuir I (1918) The adsorption of gases on plane surfaces of glass, mica, and platinum J American Chem Society 40:1361
- Meilanov RP, D.A Sveshnikova, Shabanov OM (2002) Fractal nature of sorption kinetics J Phys Chem A 106:11771–11774 doi:10.1021/jp0216575
- Mohan D. Pant, Headrick TC (2013) A Method for Simulating Burr Type III and Type XII Distributions through L-Moments and L-Correlations Hindawi Publishing Corporation ISRN Applied Mathematics 2013:14 doi:org/10.1155/2013/191604

- Naidoo R et al. (2012) Surface-immobilization of chromatographically purified bacteriophages for the optimized capture of bacteria *Bacteriophage* 2:15-24 doi:10.4161/bact.19079
- Ncibi M, Altenor S, Seffen M, Brouers F, Gaspard S (2008) Modelling single compound adsorption onto porous and non-porous sorbents using a deformed Weibull exponential isotherm *Chem Eng J* 145:196-202
- Ncibi MC, Mika S (2015) Optimized removal of antibiotic drugs from aqueous solutions using single, double and multi-walled carbon nanotubes *J Hazard Mater* 298:102-110 doi:org/10.1016/j.jhazmat.2015.05.025
- Pereira LM (2010) Fractal Pharmacokinetics *Comput Math Methods in Med* 11:161-184 doi:10.1080/17486700903029280
- Robledo A, Moyano LG (2008) q-deformed statistical-mechanical property in the dynamics of trajectories en route to the Feigenbaum attractor *Physical Review E* 77:036213 doi:10.1103/PhysRevE.77.036213
- Sandro A, Betty Carene, Evens Emmanuel, Jacques Lambert, Jean-Jacques Ehrhardt, Gaspard S (2009) Adsorption studies of methylene blue and phenol onto vetiver roots activated carbon prepared by chemical activation *J Hazard Mater* 165:1029–1039 doi:10.1016/j.jhazmat.2008.10.133
- Selmi T et al. (2018a) Tetracycline removal with activated carbons produced by hydrothermal carbonisation of *Agave americana* fibres and mimosa tannin *Ind Crops Prod* 115:146-157 doi:<https://doi.org/10.1016/j.indcrop.2018.02.005>
- Selmi T, Seffen M, Brouers F, Fierro V, Sammouda H (2018b) Adsorption of Model Dyes Onto Porous Materials: Effect of pH and Temperature on the Parameters of Brouers-Sotolongo Kinetic Fractal and Generalized Isotherm. In: Kallel A, Ksibi M, Ben Dhia H, Khélifi N (eds) *Recent Advances in Environmental Science from the Euro-Mediterranean and Surrounding Regions: Proceedings of Euro-Mediterranean Conference for Environmental Integration (EMCEI-1), Tunisia 2017*. Springer International Publishing, Cham, pp 1039-1041. doi:10.1007/978-3-319-70548-4\_299
- Selmi T, Seffen M, Sammouda H, Sandrine M, Jagiello J, Celzard A, Fierro V (2018c) Physical meaning of the parameters used in fractal kinetic and generalised adsorption models of Brouers–Sotolongo *Adsorption* 24:11-27 doi:10.1007/s10450-017-9927-9
- Sips R (1948) The Structure of a Catalyst Surface *J Chem Phys* 16:490-495 doi:org/10.1063/1.1746922

- Sotolongo-Grau. O, Rodríguez-Pérez. D, Antoranz. J. C, Sotolongo-Costa. Oscar (2010) Tissue Radiation Response with Maximum Tsallis Entropy Phys Rev Lett 105:158105
- Sotolongo-Grau. O, Rodriguez-Perez. D, Sotolongo-Costa. O, Antoranz. J. C (2013) Tsallis entropy approach to radiotherapy treatments Phys A: Stat Mech Appl 392:2007-2015 doi:<https://doi.org/10.1016/j.physa.2013.01.020>
- Stanislavsky A, Weron K (2013) Is there a motivation for a universal behaviour in molecular populations undergoing chemical reactions? Phys Chem Chem Phys 15:15595-15601 doi:10.1039/C3CP52272E
- Temkin MI (1941) Adsorption equilibrium and kinetics of process on non homogeneous surfaces and in the interaction between adsorbed molecules J Phys Chem 15:296-233
- Tonkin JA, Shamsudeen S, Martyn RB, Rita ES, Paul R, Huw DS (2014) Optical tracking of drug release from porous silicon delivery vectors The Institution of Engineering and Technology Optoelectronics 8:113-116 doi: <http://dx.doi.org/10.1049/iet-opt.2013.0080>
- Tsallis C (2009) Nonadditive entropy and nonextensive statistical mechanics -an overview after 20 years Brazilian Journal of Physics 39:337-356 doi:<http://dx.doi.org/10.1590/S0103-97332009000400002>
- Volesky B (2007) Biosorption and me Water Res 41:4017-4029 doi:<https://doi.org/10.1016/j.watres.2007.05.062>
- Weber WJ, Morris JC (1963) Kinetics of adsorption on carbon from solution J Sanitary Eng Div 89:31-60
- Wu F-C, Tseng R-L, Juang R-S (2009) Characteristics of Elovich equation used for the analysis of adsorption kinetics in dye-chitosan systems Chem Eng J 150:366-373 doi:<https://doi.org/10.1016/j.cej.2009.01.014>

## Figure caption

Figure 1: Effect of contact time and initial concentration on: (a) MB at pH 8; and (b) MO at pH 2.5 onto F300 at 25°C (lines are just guides for the eye).

Figure 2: Effect of pH and temperature on the adsorbed amount onto F300 of: (a) MB; and (b) MO, both at  $C_0=10$  mg/L.

Figure 3: Effect of pH and temperature on the free energy of adsorption  $\Delta G^\circ$  onto the four ACs of: (a) MB; and (b) MO, both at  $C_0=10$  mg/L.

Figure 4: Effect of pH on: (a and b) standard adsorption enthalpy  $\Delta H^\circ$ ; and (c and d) on standard adsorption entropy  $\Delta S^\circ$  for: (a and c) MB; and (b and d) MO onto the four ACs.

Figure 5: BSf (1, $\alpha$ ) kinetics model applied to the adsorption of: (a,b) MB; and (c,d) MO onto F300 for different pH and temperatures, using an initial dye concentration  $C_0=10$  mg/L.

Figure 6: Variation with pH and temperature of BSf (1, $\alpha$ ) parameters: (a)  $\tau_C$ ; and (b)  $\alpha$ , for the adsorption onto F300 of MB and MO (both at  $C_0=10$  mg/L).

Figure 7: Fits of the BG isotherm to the adsorption data onto F300 of: (a and b) MB; and (c and d) MO, for different temperatures and pH.

Figure 8: Variation with pH and temperature of BG parameters,  $a$  and  $b$ , determined by adsorption of: (a and c) MB; (b and d) MO, onto F200, F300, Acticarbone® and Cecalite®.

## List of table

Table 1 : Characteristics of the four ACs used herein (Selmi et al. 2018c): surface area ( $S_{BET}$ ), total pore volume measured by nitrogen adsorption at  $-196^{\circ}\text{C}$  ( $V_{tot}$ ), total amount of surface functional groups, and pH at the point of zero charge ( $pH_{PZC}$ ).

Table 2: Kinetic models derived from the BSf kinetic model

Table 3: Adsorption isotherms models derived from the GBS isotherm.